

# INTERTWINED FANO RESONANCES IN SUB-WAVELENGTH METALLIC GRATINGS: OMNIDIRECTIONAL AND WIDEBAND OPTICAL TRANSMISSION: SUPPLEMENTAL DOCUMENT

This document provides supplementary information to "Intertwined Fano resonances in sub-wavelength metallic gratings: omnidirectional and wideband optical transmission". It includes the pole-zero study in the complex plane for the slit, SG and GSG structures. Magnetic field maps are also provided at the zero and poles frequencies for the SG and GSG structures. Finally, properties of other structures, based on the same principle but designed for other wavelengths, are presented.

## I. POLE-ZERO STUDY

Figure 1 shows the transmission coefficient (value and phase) as a function of a complex wavelength of incidence. This complex study gives complete information about the structure, because the poles (divergent transmission) and zeros (zero transmission) fully characterize its resonant behavior. The structure's transmission spectrum is thus a "slice" of this 2D map, along the real axis. Figure. 1c) shows this study for the full structure, while Figure. 1b) shows it for only the first slit+groove combination and Figure. 1a) shows it for the slit alone. The phase map of the transmission coefficient is particularly useful, as the phase jump (visible by a sudden contrast) draws a line between linked poles and zeros, and also makes visible the existence of zeros out of the computation domain. How much the zero-phase region is tilted near the real axis is also a good prediction of how sharp the Fano resonance will be.

Comparison between these shows that the addition of a groove does not have a completely straightforward effect. Indeed, it does not simply add a pole-zero combination, otherwise the slit pole at  $\lambda = 8.8 + 1.2j \mu\text{m}$  on Fig. S1a) would not be shifted to  $\lambda = 8.5 + 1.7j \mu\text{m}$  for SG1 (on Fig. S1b)) or to  $\lambda = 8 + j \mu\text{m}$  for GSG (on Fig. S1c)). Indeed, there is a coupling between the slit mode and the groove modes which leads to two new poles each time a groove is added.

This means that the interferential interpretation is a bit simplistic: the transmission peak (resp. dip) cannot only be explained by the fact that the groove and slit modes' reflection interfere destructively (resp. constructively) at a given wavelength. The Fano profiles, however, are very well predicted by this complex mode study: the poles and zeros, not being symmetric with respect to the real wavelength axis, lead to quick variations of the spectrum.

### A. Fano parameter analysis

The  $q$  Fano parameter is the best description of the asymmetry of the spectrum ([1]), and can be given by ([2]):

$$q = -\cot\left(\frac{1}{2} \arcsin\left[\frac{-2\text{Im}(\omega_r)}{\omega_p - \omega_d}\right]\right) \quad (1)$$

with  $\omega_r$  the complex resonant frequency, and  $\omega_{p,d}$  the real frequency of the pole/dip.

This analysis leads to:

- $q \simeq -1.17$  for SG1

- $q \simeq 1.02$  for SG2

The difference in sign corresponds to the fact that the zero appears before or after the peak. The proximity of the values account for the symmetry of the final profile.

### B. Field intensity maps

Figures 2 and 3 show field intensity (precisely:  $|H_y|$ ) maps at the poles and zeros identified in Fig. 1b) for the SG1 structure. They show clearly a very low field intensity in the slit at the transmission zeros. (at least one order of magnitude lower than at the poles). Furthermore, a high field intensity can be observed in the grooves at most poles. This can hint at one of the device's limitation: strong resonance in a metallic groove leads to losses by absorption in the metal. This can probably explain why the transmission maximum reaches 90% but no higher.

Figures 4 and 5 show similar field maps for the poles and zeros identified on Fig 1c), for the GSG structure. The behavior is similar to that observed on Figs S2 and S3 : high intensities in both a groove and the slit for poles, lower field intensities localized mostly in the grooves for zeros.

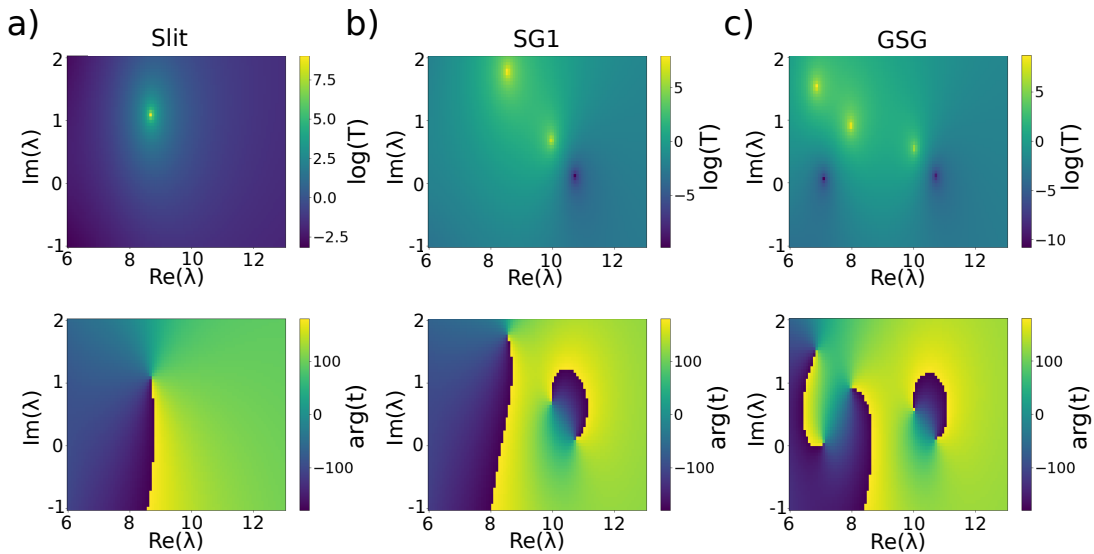


FIG. 1. Amplitude and phase of the transmission in the complex plane for a) the slit, b) the  $\text{SG}_1$  structure and c) the GSG structure.

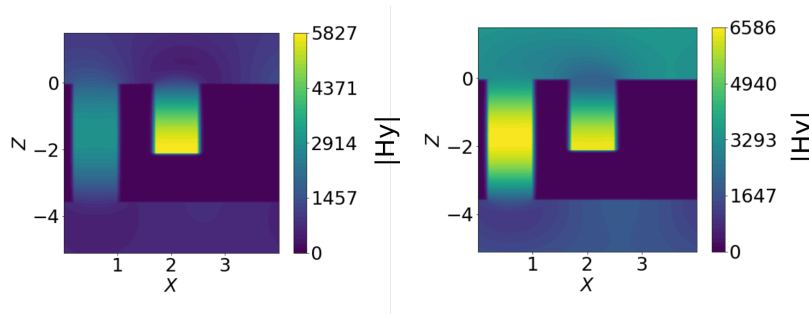


FIG. 2. Magnetic field of the slit-groove (SG) structure at the two pole frequencies at  $\lambda_p = 10.0 + 0.7j \mu\text{m}$  and  $\lambda_p = 8.5 + 1.8j \mu\text{m}$

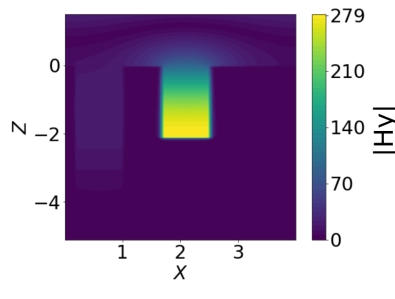


FIG. 3. Magnetic field of the slit groove structure at  $\lambda_0 = 11 \mu\text{m}$

## II. ALTERNATIVE GSG STRUCTURES

### A. Structures for other spectral ranges

#### B. GSG structures on a substrate

Figure 6 shows the wavelength-incidence plots of structures designed for other working regimes in the infrared and terahertz range (4-5  $\mu\text{m}$  band, 10-12  $\mu\text{m}$  band, 200-250  $\mu\text{m}$  band). They are obtained through a direct scaling of the main

article's structure (the scaling factor is 0.45, 1.2 and 25, respectively). These results show that the scaling of the structure is a simple way to shift its spectral behavior.

Fig. 7 shows both the wavelength-incidence plot and transmission spectrum of a structure with a 300  $\mu\text{m}$  thick substrate of  $\text{CaF}_2$ . No antireflective coating is added. The plots show that the overall properties of the structure are conserved.

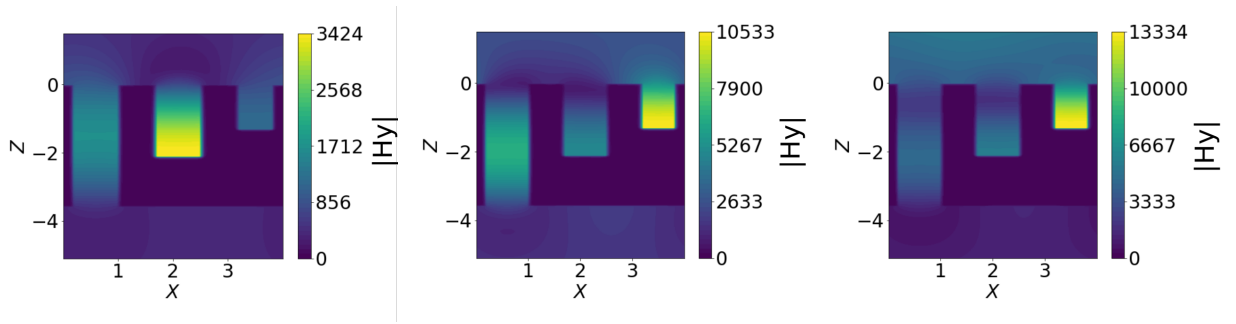


FIG. 4. Magnetic field of the GSG structure at the three poles at  $\lambda_p = 10 + 0.6j \mu\text{m}$ ,  $\lambda_p = 8.0 + 0.9j \mu\text{m}$  and  $\lambda_p = 6.8 + 1.5j \mu\text{m}$

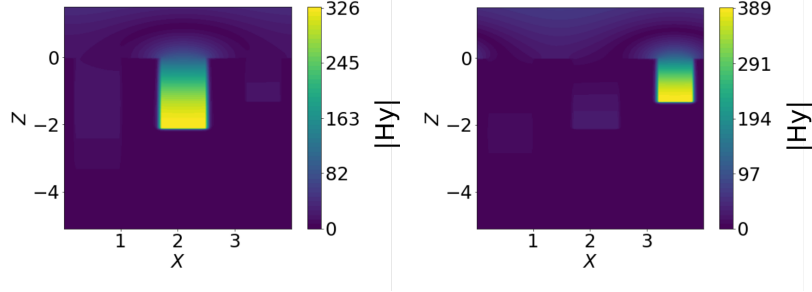


FIG. 5. Magnetic field of the GSG structure at the two zeros occurring at  $\lambda_0 = 10.6 \mu\text{m}$  and  $\lambda_0 = 7.0 \mu\text{m}$

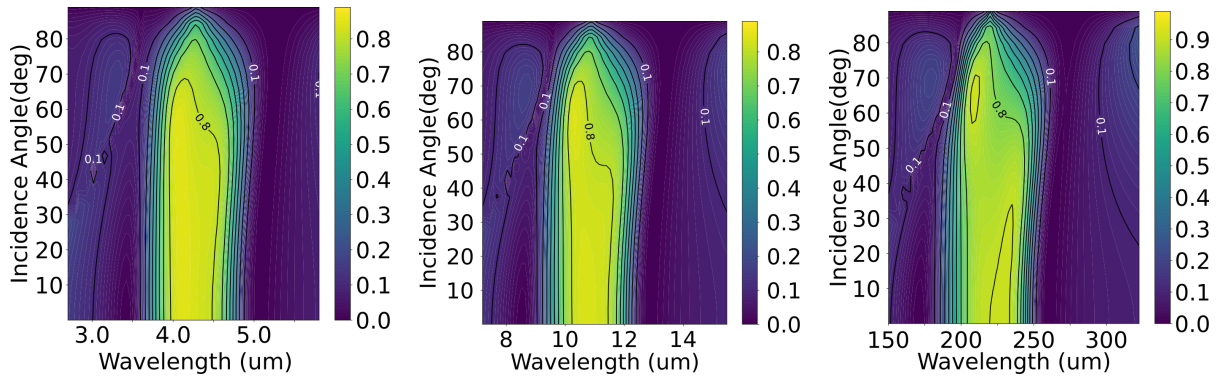


FIG. 6. (left) 3-5  $\mu\text{m}$  structure (dimensions:  $w_s = 0.36 \mu\text{m}$ ,  $w_1 = 0.36 \mu\text{m}$ ,  $w_2 = 0.24 \mu\text{m}$ ,  $h_s = 1.62 \mu\text{m}$ ,  $h_1 = 0.94 \mu\text{m}$ ,  $h_2 = 0.58 \mu\text{m}$  and period  $L = 1.8 \mu\text{m}$ ), (center) 10-12  $\mu\text{m}$  structure (dimension:  $w_s = 0.96 \mu\text{m}$ ,  $w_1 = 0.96 \mu\text{m}$ ,  $w_2 = 0.72 \mu\text{m}$ ,  $h_s = 4.32 \mu\text{m}$ ,  $h_1 = 2.52 \mu\text{m}$ ,  $h_2 = 1.56 \mu\text{m}$  and period  $L = 4.8 \mu\text{m}$ ), (right) THz structure (dimensions:  $w_s = 20 \mu\text{m}$ ,  $w_1 = 20 \mu\text{m}$ ,  $w_2 = 15 \mu\text{m}$ ,  $h_s = 90 \mu\text{m}$ ,  $h_1 = 25.5 \mu\text{m}$ ,  $h_2 = 32.5 \mu\text{m}$  and period  $L = 100 \mu\text{m}$ ).

- [1] M. F. Limonov, M. V. Rybin, A. N. Poddubny, and Y. S. Kivshar, Fano resonances in photonics, *Nature photonics* **11**, 543 (2017).  
 [2] V. Grigoriev, S. Varault, G. Boudarham, B. Stout, J. Wenger, and

N. Bonod, Singular analysis of fano resonances in plasmonic nanostructures, *Physical Review A* **88**, 063805 (2013).

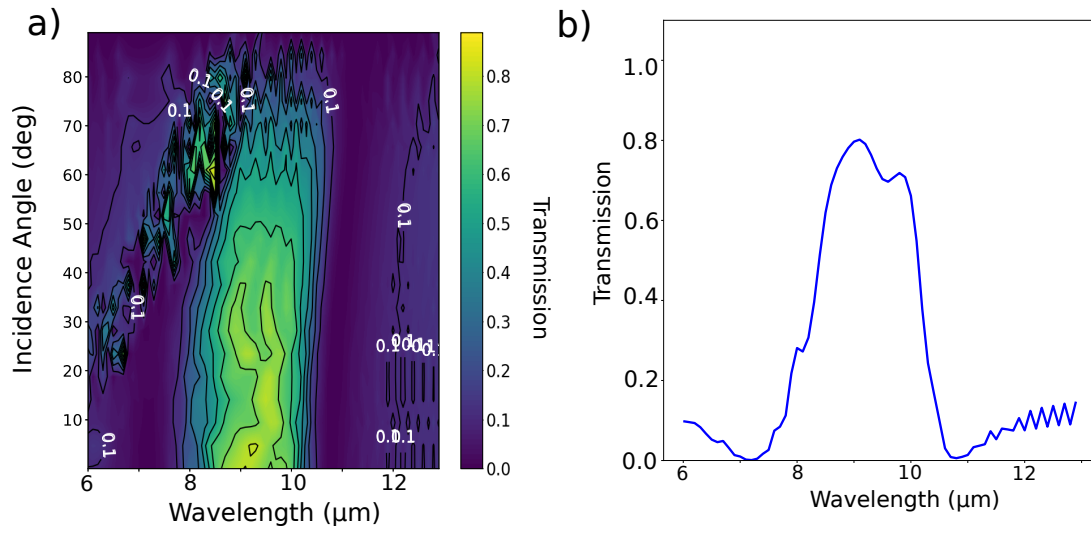


FIG. 7. Structure with substrate: same dimensions as the main article's structure, with a 300  $\mu\text{m}$  substrate of CaF<sub>2</sub>